ELSEVIER

Journal of Hydrology 259 (2002) 236–245

Journal of Hydrology

www.elsevier.com/locate/jhydrol

An NMR study of single- and two-phase flow in fault gouge filled fractures

Q. Chen[a,b], W. Kinzelbach[a,*]

[a]*Swiss Federal Institute of Technology Zurich, Institute of Hydromechanics and Water Resources Management, ETH-Hoenggerberg, CH-8093 Zurich, Switzerland*

[b]*Institute of Porous Flow and Fluid Mechanics, China National Petroleum Corporation and Chinese Academy of Sciences, P.O. Box 44, Langfang, Hebei, 065007, People's Republic of China*

Received 29 June 2001; revised 12 November 2001; accepted 23 November 2001

Abstract

The characteristics of single- and multiphase flow through fractured rock are of considerable interest in petroleum and natural gas exploitation as well as in the risk assessment of underground repositories. Flow processes of water and gas were studied in a granite core containing a fault gouge filled fracture zone. The pore structure of the sample was scanned by X-ray computed tomography (CT).

A reversible change of fracture aperture due to shrinking and swelling of fault gouge was observed when drying, saturating and again drying the core. There is evidence that the fractures at the contact between matrix and fault gouge contribute most to permeability.

Changes in the size distribution of water filled pores were monitored by low magnetic field nuclear magnetic resonance (NMR) during miscible flooding with deuterated water and immiscible flooding with nitrogen gas. Gas breakthrough occurred quickly at extremely low gas saturation indicating preferential pathways. Water saturation decreased gradually with the increase of injection pressure. In comparison, the process of miscible flooding showed a much more homogeneous behavior. Deuterated water breakthrough occurred slowly and at higher deuterated water saturation. In miscible flooding, the large and small range of the pore size distribution decreased simultaneously indicating that deuterated water invaded both types of pores at the same time. In the immiscible flooding process, the large pores were preferentially invaded by gas. At low water saturation, water only fills the very small pores, which do not contribute to gas flow.

Keywords: Nuclear magnetic resonance; Flow in fractures; Fault gouge; Miscible flooding; Immiscible flooding

1. Introduction

Fluid flow and transport in fractured porous media have commonly been described by the parallel plate model (Iwai, 1976; Witherspoon et al., 1980). This assumes that the aperture variability is small compared to the mean aperture, and a single fracture can be modeled with a spatially constant mean aperture. However, real fracture surfaces are not smooth and parallel but are rough and contact each other at discrete points (Brown and Scholz, 1985; Brown, 1995). The aperture variability can potentially have profound impacts on the hydraulic and solute transport behavior of a fracture (Silliman, 1989). Flow in open fractures with spatially varying apertures has

* Corresponding author. Tel.: +41-1633-3066; fax: +41-1633-1061.

E-mail addresses: quanchen@163bj.com (Q. Chen), kinzelbach@ihw.baug.ethz.ch (W. Kinzelbach).

0022-1694/02/$ - see front matter
PII: S0022-1694(01)00599-6

been studied extensively (Olsson et al., 1993; Brown et al., 1995; Walsh et al., 1997). Fluid flow and solute transport in fractures filled with fault gouge, a fine-grained material produced by shear of the fractures, are significantly different from the open fracture phenomena. Few papers discuss flow in fault gouge filled fractures. In this paper, the fluid flow and transport of miscible and immiscible displacement in a fault gouge filled fracture is for the first time investigated by NMR. The characteristic changes in pore size distribution filled by water were studied using low magnetic field NMR relaxation time distributions.

2. NMR measurement of saturated pore size distribution

The essential information on rocks or sedimentary samples, which can be provided by low-field NMR, is the size distribution of fluid filled pores. It is shown in the following how this distribution and the NMR signal are related to each other. The advantage of NMR is that the pore size distribution filled by fluid is determined non-intrusively and can be observed during multiphase flow through porous media. Hydrogen nuclei have a magnetic moment and behave like small bar magnets. When subjected to a magnetic field, such nuclei tend to align their magnetic moments parallel to the field, producing a net nuclear magnetization. In the NMR method, their angle with respect to the magnetic field is changed by a radio frequency pulse. Once the pulse stops they regain their original orientation by relaxation. In a saturated porous medium, the relaxation time depends not only on the fluid but also on the medium and the interaction between both of them. Thus the study of relaxation time can provide information on the structure of a porous medium.

Pulsed NMR measures the magnetization (M) and transverse relaxation time (T_2) of hydrogen nuclei contained in the pore fluids. M is proportional to the number of hydrogen nuclei in the sensitive region and can be scaled to give an NMR porosity (Timur, 1969; Kenyon, 1992). In a porous medium, the fluid interacts with the rock surface, which promotes NMR relaxation. Therefore for fluids confined in pores, the T_2 value can be shorter than that of the bulk fluid (Korringa et al., 1962; Kenyon, 1992). Three different mechanisms operate in parallel and contribute to the overall apparent relaxation rate $1/T_{2A}$ of fluid in porous media (Kleinberg and Horsfield, 1990; Kleinberg et al., 1993).

$$1/T_{2A} = 1/T_{2B} + 1/T_{2S} + 1/T_{2D} \quad (1)$$

where the subscripts A, B, S, and D denote apparent, bulk, surface-induced, and diffusion-induced mechanisms, respectively. The bulk relaxation time, T_{2B}, is a property of the fluid only. Because the relaxation time of water in rocks is much shorter than the relaxation time of bulk water, the bulk terms in the Eq. (1) can be neglected. The surface-induced relaxation, characterized by T_{2S}, is due to interaction between fluid and the solid surface, while the diffusion related relaxation, characterized by T_{2D}, is caused by diffusion in the inhomogeneous magnetic field arising from the magnetic susceptibility contrast between the grains and pore fluid. The surface and diffusion induced relaxation rates are given by (Fukushima and Roeder, 1981; Cohen and Mendelson, 1982)

$$1/T_{2S} = \rho_2 S/V \quad (2)$$

$$1/T_{2D} = ((\gamma G T_E)^2 D_o)/12 \quad (3)$$

where ρ_2 is the surface relaxivity, S/V the surface-to-volume ratio, γ the gyromagnetic ratio, G the 'background' magnetic field gradient, T_E the echo time, and D_o is the self-diffusion coefficient of the liquid.

The majority of rocks conforms to the 'fast-diffusion' (Brownstein and Tarr, 1979) or 'surface limited' (Belton et al., 1988) relaxation regime in which the rate limiting step is relaxation at the surface, not the transport of magnetization to the surface. Thus the spins experience a rapid change of environments and the local fields in each region of a pore are averaged to their mean value. As a consequence, a single exponential decay is observed for a given pore, and the rate of magnetization decay depends on surface-to-volume ratio only (Kleinberg et al., 1994). Under the conditions of low magnetic field strength (i.e. G is also small) and short T_E (Kleinberg and Horsfield, 1990; Kleinberg et al., 1993), the enhancement in T_2 decay coming from diffusion in the inhomogeneous local magnetic fields is negligible compared to the surface relaxation mechanism.

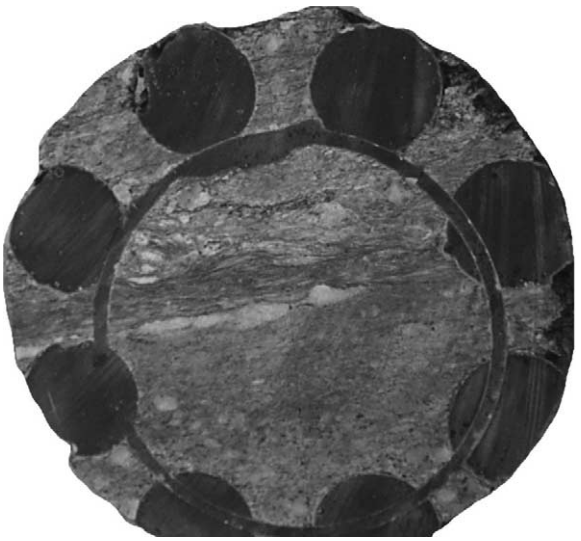

Fig. 1. Section face of the core at inlet side.

Therefore, the measured T_2 values are given by

$$1/T_{2A} = \rho_2 S/V \quad (4)$$

Eq. (4) forms the basis of NMR core analysis and log interpretation: T_2 is proportional to V/S, which in turn is proportional to pore size. This means that in small pores relaxation is faster than in large pores. Note that this result is made possible by using a low magnetic field, which avoids disturbances by paramagnetic properties of natural materials seen in high-field NMR. The price paid is the loss in spatial resolution.

In the measurement, the CPMG pulse sequence proposed by Carr and Purcell, 1954, Meiboom and Gill, 1958, was used. It consists of one 90° pulse followed by a series of 180° pulses. The time interval between two 180° pulses is the echo time T_E, the time between two sequences is the recovery time T_R. T_R must be long enough to make sure that magnetization recovery to equilibrium is efficient. When hydrogen nuclei are tipped 90° from the direction of the magnetic field, they precess and dephase due to the inhomogeneity of the magnetic field. The nuclei can be refocused after a 180° pulse is transmitted. As the nuclei rephase, they generate a signal in a receiving coil—a spin echo (Hahn, 1950). The 180° pulses can be applied repeatedly to produce a series of echo trains.

The total measured magnetization signal is a superposition of the signals coming from all pores within the measurement volume. It can be expressed as a sum of exponentials

$$M(t) = \sum_i A_i(0) \exp(-t/T_{2i}) \quad (5)$$

That means the overall decay is the sum of the individual decays and reflects pore size distribution. By using proper fitting routines Eq. (5) can be inverted into a T_2 relaxation time distribution, where the T_{2i} belongs to a preselected basis set of relaxation time constants and $A_i(0)$ are the signal amplitudes (Dunn and Latorraca, 1994; Bulter and Dawson, 1981). Because T_2 depends linearly upon pore size, the T_2 distribution corresponds to a pore size distribution.

3. Experimental procedures

3.1. Core drilling and processing

A granite sample containing a fault gouge filled mylonitic fracture zone was taken from a shear zone (VE tunnel, location 422.30 m) at the Grimsel test site, Switzerland. The fault gouge consists of materials finely ground due to friction in the phyllosilicate-rich mylonite bands. In situ sealing by epoxy resin and drilling parallel to fracture planes were performed in order to not disturb the fault gouge filled fracture zone. For fixing the rock sample in situ, eight bore holes distributed uniformly along the circumference of a circle with diameter 124 mm were drilled by a drill bit with outer diameter 32 mm and inner diameter 28 mm to a depth of about 40 cm. During drilling, fresh water was used as coolant. After completion of the drilling, epoxy resin was filled into the boreholes. A high viscosity resin was used in order to prevent the penetration of resin into the fracture zone. To avoid breaking during coring, after hardening of the epoxy resin in the boreholes, the inner annulus was drilled by a drill bit with outer diameter 106 mm and inner diameter 99 mm to a depth of about 40 cm. Only little fresh water was used for cooling in order to not wash out fault gouge from the sample. High viscosity epoxy resin was poured into the annulus. After hardening of the epoxy resin, the outer annulus was drilled using a drill bit with outer diameter 158 mm and inner diameter

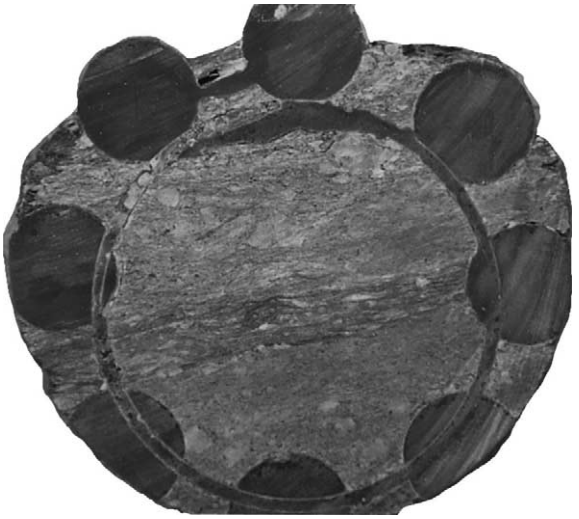

Fig. 2. Section face of the core at outlet side.

150 mm to a depth of about 70 cm. During drilling fresh water was used as coolant. Finally, the core sample was broken at a depth of about 70 cm.

The faces of the core were sawed while cooling with liquid nitrogen in order to avoid loss of fault gouge material. The final length of the sample was 17 cm. The two faces of the core are shown in Figs. 1 and 2.

A small granite matrix sample for the measurement of matrix properties was drilled by a drill bit with inner diameter of 1 in. from the cut-away part of the core.

For measurement of permeability and porosity, the samples were dried at 40 °C for more than 1 week until the weight of the samples remained constant.

3.2. Pore structure analysis by CT scan

X-ray computed tomography (CT) technology (Mogen, 1983) provides the capability of non-destructive visualization and analysis of the internal structure of rock materials.

CT images are created by measuring the attenuation of a collimated X-ray beam after its passage through a given substance. The sample attenuates the X-ray beam in an exponential manner according to Beer's law:

$$I = I_o \, e^{-\mu X} \tag{6}$$

where I_o and I represent the intensity of the X-ray beam before and after passage through the sample, respectively, X is the path length and μ is defined as the linear attenuation coefficient. The attenuation coefficient μ for the sample is a function of the atomic number (Z) and the bulk density (ρ) of the substance and is given by

$$\mu = \rho(a + bZ^{3.8}/E^{3.2}) \tag{7}$$

where a is the Klein–Nishima coefficient, b the constant, and E is the photon energy of the X-ray. Variations of density and chemical composition in a rock sample are reflected in 2D CT images by gray-scale contrasts.

The core was scanned under different conditions by computed tomography (Bio-Imaging Research, Inc. ACTIS 420/600 X-ray computerized tomographic system) using 420 keV tube voltage and 5.0 mA tube current. The minimum slice thickness is 0.25 mm and the maximum imaging matrix is 1024 × 1024 pixels. The dry core was saturated under vacuum conditions and scanned by CT. Then the core was dried and scanned again.

3.3. Gas permeability and porosity measurements

To prepare the core for flow experiments the material beyond the inner resin annulus (diameter 107 mm) was cut away. Then the core annulus was molded by epoxy resin in a mold tool with outer diameter 110 mm to fit the core holder.

Gas permeability according to Darcy's law was measured. Core samples were held in a Hassler core holder by a confining pressure of 1.8 MPa. Nitrogen gas was injected into the core from the inlet by a pressurized cylinder. The gas pressure, p_1, was measured by a pressure manometer connected to the inlet. The volume rate of gas flow, Q_o, was measured by a soap film flowmeter connected to the outlet, which was under atmospheric pressure. Gas permeability, K_g, was calculated as follows

$$K_g = 2\mu_g Q_o L/A(p_1^2 - p_0^2) \tag{8}$$

where μ_g is the gas viscosity, Q_o the atmospheric pressure, and L and A are the length and the cross sectional area of the core sample, respectively. Klinkenberg permeability (K_∞) was calculated by linear regression between K_g and the reciprocal of

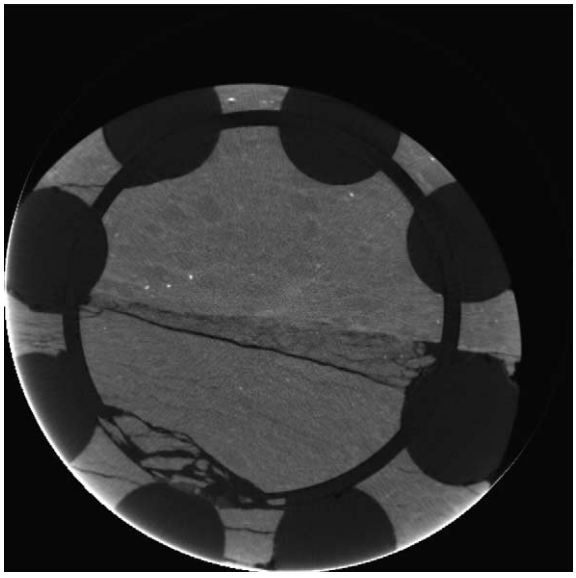

Fig. 3. Dry core scanned by CT (transverse), position at center of core (slice thickness 0.25 mm, resolution 0.3 mm/pixel).

the average pressure, $p_a = (p_1 + p_0)/2$, extrapolating to infinite average pressure (Klinkenberg, 1941).

After gas permeability measurements, core samples were saturated with distilled water under vacuum conditions. The total porosity of the core samples was measured using Archimedes' law.

3.4. Miscible flooding

On the saturated core, miscible flooding was conducted using deuterated water under two different constant flux conditions (1 and 4 ml/min). The process of miscible flooding was monitored by NMR. As deuterium does not produce a magnetic resonance signal under the hydrogen nucleus (H^1) resonance frequency, it can serve as a tracer. Pores filled with deuterated water will vanish from the pore size spectrum obtained by NMR.

NMR relaxation measurements were carried out on a home made NMR spectrometer with a magnetic field strength of 1175 G, corresponding to a resonance frequency of 5 MHz of the hydrogen nucleus (H^1). The permanent magnet has a 13 cm bore in horizontal direction. A 12 cm probe was used. The experimental parameters were as follows: echo time 240 μs, recovery time 4000 ms, number of scans 32, number of echoes 1024.

The volume of the production liquid was measured by test tube. Then the percentage of deuterated water in the test tube was analyzed by Bruker Biospec 47/40 superconductive NMR spectrometry in order to calculate the average water saturation in the core during deuterated water flooding. The strength of the magnetic field is 4.7 T, which corresponds to 200 MHz for the hydrogen nucleus (H^1) resonance frequency.

3.5. Immiscible flooding

Immiscible flooding was performed by injecting nitrogen gas into the saturated core under different pressure conditions. First, a gas threshold pressure test was performed to determine the gas entry pressure into the water-saturated core. The observed threshold pressure corresponds to a maximum capillary radius according to Laplace's equation.

$$P_c = 2\sigma \cos\theta / r \tag{9}$$

In the equation, σ is the interfacial tension, θ the contact angle and r the pore throat radius. Under the conditions of this experiment, where water and nitrogen gas are used, the following values are valid: $\sigma = 72$ m N/m, $\theta = 0$.

The process of gas flooding was also monitored by NMR. Nitrogen gas filled pores do not produce an NMR signal at the resonance frequency of protons. Therefore, they vanish from the pore size spectrum obtained by NMR.

Gas permeability, K_g, was measured at different water saturations under steady state conditions. The gas flow rate for the measurement of permeability was kept low in order to stay within laminar flow conditions. Different water saturations were established by stepwise increase of the pressure of gas displacement until the irreducible water saturation was reached. Afterwards, an evaporation method was used to decrease water saturation again. The sample was sealed in a plastic bag and placed in cold storage for a week to obtain hydrodynamic equilibrium within the core. The core was weighed at different water contents in order to calculate water saturation.

Gas relative permeability, K_{rg}, was calculated by the formula

$$K_{rg} = K_g / K_\infty. \tag{10}$$

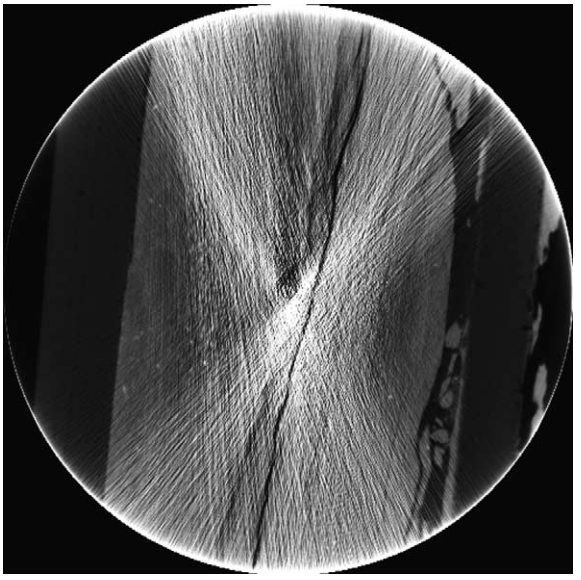

Fig. 4. Dry core scanned by CT (sagittal), position vertical to fracture (slice thickness 0.25 mm, resolution 0.30 mm/pixel) (diagonal lines are artefacts).

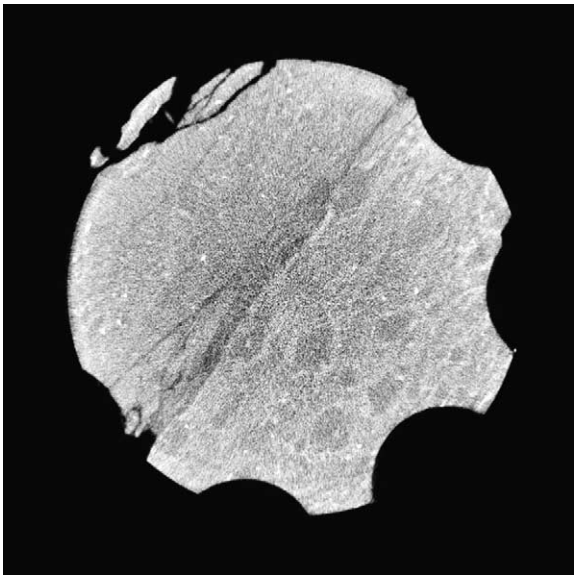

Fig. 5. Water-saturated core scanned by CT (transverse), position at center of core (slice thickness 0.25 mm, resolution 0.25 mm/pixel).

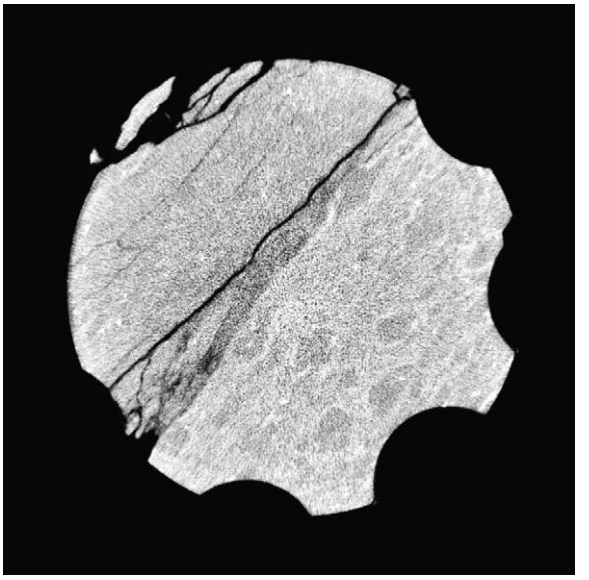

Fig. 6. Dry core (after second drying) scanned by CT (transverse), position at center of core (slice thickness 0.25 mm, resolution 0.25 mm/pixel).

4. Results and discussion

4.1. Pore structure from CT scans

An example of a CT scan of the dried core at the center section is shown in Fig. 3. Other scanned cross sections show a very similar picture, with a pronounced open fracture along the fault gouge filling. This fracture is continuous through the whole core as can be seen in Fig. 4. The following parameters were obtained by image processing and calculation: the total cross sectional area of the core (A) is 71.9951 cm^2, the fraction of fault gouge layers (A_f) is 15.7%.

4.2. Gas permeability and porosity

The Klinkenberg permeability (K_∞) is 144.8×10^{-3} μm^2, and the permeability of the granite matrix sample (K_m) is 2.4×10^{-6} μm^2. The permeability of the fault gouge layer (K_f) of 922.3×10^{-3} μm^2 is then calculated from the equation

$$K_\infty = K_m(1 - A_f) + K_f A_f \quad (11)$$

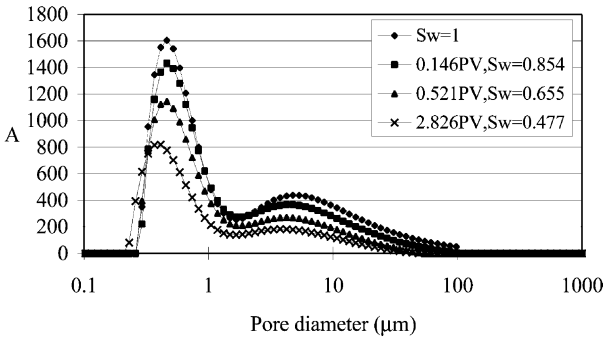

Fig. 7. Variation of pore size distribution filled by water during miscible flooding by deuterated water.

where K_m is the matrix permeability, K_f the permeability of the fault gouge layer, and A_f is the area fraction of the fault gouge layer with respect to the total area of the core face as determined from CT scanning.

The permeability (K_w) determined under water-saturated conditions using Darcy's law is $109.7 \times 10^{-3}\ \mu m^2$. It differs considerably from the gas permeability.

The total porosity (ϕ) of the core is 3.32% while the porosity of the granite matrix sample (ϕ_m) is 1.1%. This leads to a porosity of the fault gouge layer (ϕ_f) of 15.2%, according to the equation

$$\phi = \phi_m(1 - A_f) + \phi_f A_f \quad (12)$$

where ϕ is the total porosity of the core, ϕ_m the matrix porosity, and ϕ_f is the porosity of the fault gouge layer. With respect to the total volume of the core, the percentage of the matrix pore volume is 28%, and the contribution by the fault gouge layers is 72%.

4.3. Pore structure changes

CT scan measurements were compared for three different conditions: dry sample before cutting (Figs. 3 and 4), water-saturated sample (Fig. 5), and sample dried again (Fig. 6). Only the center cross section is shown, with other cross sections showing the same behavior. Reversible changes of fracture aperture under the three conditions were observed. The fracture aperture becomes smaller after saturation by water due to swelling and dispersion of fault gouge. After drying the core again, the fracture apertures almost recover to the original values due to the shrinking of fault gouge. The changes of pore structure between the dry and saturated states are the reason for the difference in water permeability and Klinkenberg permeability. The fractures at the contact between matrix and fault gouge contribute much more to permeability than the pores within the fault gouge. Therefore, experiments based on the dried core

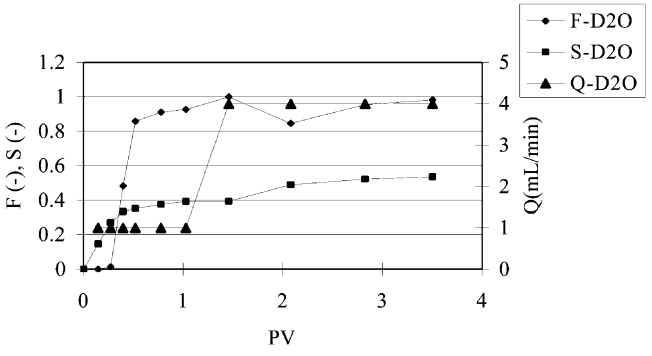

Fig. 8. Deuterated water injection rate (Q-D2O), deuterated water saturation (S-D2O), and deuterated water production fraction (F-D2O) shown as functions of the injected pore volume (PV) of deuterated water.

Table 1
Gas flooding pressure and corresponding equilibrium water saturations

S_w (%)	P (kPa)
85.4	3.187
76.2	30.401
66.8	39.227
61.4	1178.765

cannot be used to evaluate the properties of the saturated fault gouge zone. Interestingly, drying may take place under high-level waste repository conditions and therefore may be relevant for nuclear safety considerations.

4.4. Miscible flooding

The experimental results of miscible displacement are presented in Figs. 7 and 8. Fig. 7 shows the water filled pore size distributions at different stages of deuterated water injection and water saturation. The pore size distribution was scaled from the T_2 distribution according to a linear relation. The proportionality constant was fixed according to the largest capillary diameter of 44.3 μm determined from the entry pressure of the saturated core of $P_t = 3.187$ kPa via Laplace's law.

The deuterated water injection rate (Q-D2O), deuterated water saturation (S-D2O) and deuterated water production fraction (F-D2O) are shown as functions of the injected pore volume (PV) of deuterated water in Fig. 8. Breakthrough of deuterated water was observed after injecting 27% of the core's total pore volume.

4.5. Immiscible flooding

The gas flooding pressures and corresponding equilibrium saturations are listed in Table 1. The irreducible water saturation is 61.4%. After each pressure step the T_2 distribution was measured by low magnetic field NMR at the corresponding saturation of the core. Gas relative permeability was obtained as a function of water saturation (Fig. 9). The gas breakthrough occurred at 98% water saturation. At a water saturation of 31% gas relative permeability is 1.

This means that at low water saturation water only fills the very small pores, which do not contribute to gas flow. For water saturation above 61%, strong phase interference between gas and water takes place, and gas relative permeability decreases strongly with the increase of water saturation due to swelling and dispersion of fault gouge. The water filled pore size distributions at different average water saturations are shown in Fig. 10. The pore size distribution was scaled from the T_2 distribution as already described earlier.

At low flooding pressure, corresponding to high water saturation, mainly big pores were desaturated by gas. With the increase of flooding pressure, water saturation in small pores also decreased gradually.

5. Conclusions

The permeability of the fault gouge layer is 5 orders

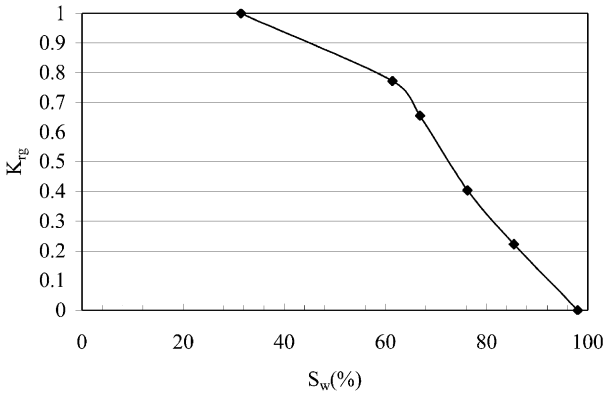

Fig. 9. Relation between water saturation S_w and gas relative permeability K_{rg}.

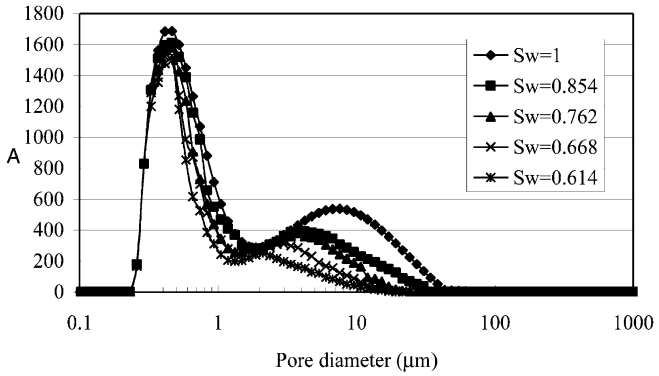

Fig. 10. Variation of pore size distribution filled by water during gas flooding (corresponding gas flooding pressures in Table 1).

of magnitude larger than that of the granite matrix. As a result, both single and multiphase flow practically take place in the fault gouge layer only.

A reversible change of fracture aperture was observed when drying, saturating and again drying the core. Fracture apertures become smaller after saturation with water due to swelling and dispersion of fault gouge. After renewed drying the fracture apertures recover almost to the original values due to shrinking of the fault gouge. The continuity of the fracture at the contact between matrix and fault gauge in the dried core suggests that this continuous feature also exists in the saturated core and is magnified by drying. It contributes decisively to the permeability of the core.

Changes in the size distribution of water filled pores monitored by low magnetic field nuclear magnetic resonance (NMR) both during miscible flooding and immiscible flooding were more homogeneous during miscible flooding than immiscible flooding. Gas breakthrough occurred quickly at extremely low gas saturation (2% of total pore volume) indicating preferential pathways. Water saturation decreased gradually with the increase of injection pressure. In comparison, the process of miscible flooding by deuterated water was much more homogeneous, deuterated water breakthrough occurring slowly at higher deuterated water saturation (27% of total pore volume).

In miscible flooding, the large and small range of the pore size distribution decreased simultaneously indicating that deuterated water invaded both types of pores at the same time. In the immiscible flooding process, the large pores were preferentially invaded by gas. At low water saturation, water fills only the very small pores, which do not contribute to gas flow. We suggest that gas is moving along preferential pathways in the core, which are identical to the fractures at the contact between granite and fault gouge seen in the CT scans in the dry state of the core.

Acknowledgements

This work was supported by NAGRA (National Cooperative for the Disposal of Radioactive Waste of Switzerland) in the framework of the GAM-project. We thank Toni Baer for assistance in in situ coring at the Grimsel Test Site, and Keith Kennedy, Paul Marschall, and Wolfgang Kickmaier for organizing the in situ coring.

References

Belton, P.S., Hill, B.P., Raimbaund, E.R., 1988. Mol. Phys. 63, 825.

Brown, R.S., 1995. Simple mathematical model of a rough fracture. J. Geophys. Res. 100, 5941–5952.

Brown, R.S., Scholz, C.H., 1985. Broad bandwidth study of the topography of natural rock surfaces. J. Geophys. Res. 90, 12575–12582.

Brown, R.S., Stockman, H.W., Reeves, S.J., 1995. Application of the Reynold's equation for modeling fluid flow between rough surfaces. Geophys. Res. Lett. 22, 2537–2540.

Brownstein, K.R., Tarr, C.E., 1979. Importance of classical diffusion in NMR studies of water in biological cells. Phys. Rev. A A19 (6), 2446–2453.

Bulter, J.P., Dawson, S.V., 1981. Estimating solution of first kind integral equations with nonnegative constraints and optimal smoothing. SIAM J. Numer. Anal. 18, 381.

Carr, H.Y., Purcell, E.M., 1954. Effect of diffusion on free precession in nuclear magnetic resonance experiments. Phys. Rev. 94, 630–638.

Cohen, M.H., Mendelson, K.S., 1982. Nuclear magnetic resonance and the internal geometry of sedimentary rocks. J. Appl. Phys. 53 (2), 1127–1135.

Dunn, K.J., Latorraca, A.G., 1994. On the calculation and interpretation of NMR relaxation time distribution, SPE28369.

Fukushima, E., Roeder, S.B.W., 1981. Experimental Pulse NMR-a Nuts and Bolts Approach. Addison–Wesley, Wokingham.

Hahn, E.L., 1950. Spin echoes. Phys Rev. 80, 580.

Iwai, K., 1976. Fundamental studies of fluid flow through a single fracture of total pore volume, PhD thesis, University of California, Berkeley.

Kenyon, W.E., 1992. Nuclear magnetic resonance as a petrophysical measurement. Nucl. Geophys. 6, 153–171.

Kleinberg, R.L., Horsfield, M.A., 1990. Transverse relaxation progresses in porous sedimentary rock. J. Magn. Reson. 88, 9–19.

Kleinberg, R.L., Straley, C., Kenyon, W.E., Akkurt, R., Farooqui, S.A., 1993. Nuclear magnetic resonance of rocks: T1 vs T2, SPE26470.

Kleinberg, R.L., Kenyon, W.E., Mitra, P.P., 1994. Mechanism of NMR relaxation of fluids in rock. J. Magn. Reson., Ser. A 108, 206–214.

Klinkenberg, L.J., 1941. The permeability of porous media to liquids and gases. Prod. Practice, 200–213.

Korringa, J., Seevers, D.O., Torrey, H.C., 1962. Theory of spin pumping and relaxation in systems with a low concentration of electron centers. Phys. Rev. 127, 1143–1150.

Meiboom, S., Gill, D., 1958. Modified spin-echo method for measuring nuclear relaxation times. Rev. Sci. Instrum. 29, 688.

Mogen, C.L., 1983. Basic Principles of Computed Tomography. University Park Press, Baltimore.

Olsson, W.A., Brown, R.S., 1993. Hydromechanical response of a fracture undergoing compression and shear. Int. J. Rock Mech. Min. Sci. Geomech. Abstr. 30, 845–851.

Silliman, S.E., 1989. An interpretation of the difference between aperture estimated from hydraulic and tracer tests in a single fracture. Water Resour. Res. 25, 2275–2283.

Timur, A., 1969. Pulsed nuclear magnetic resonance studies of porosity, movable fluid permeability of sandstones. J. Petrol. Tech. 21, 775–786.

Walsh, J.B., Brown, R.S., Durman, W.B., 1997. Effective media theory with spatial correlation for flow in a fracture. J. Geophys. Res. 102, 22587–22594.

Witherspoon, P.A., Wang, J.S.Y., Iwai, K., Gale, J.E., 1980. Validity of cubic law for fluid flow in a deformable rock fracture. Water Resour. Res. 16, 1016–1024.